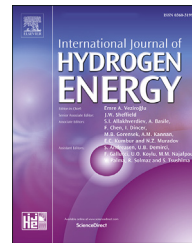




ELSEVIER

Available online at www.sciencedirect.com

ScienceDirect

journal homepage: www.elsevier.com/locate/he

Molecular dynamics simulation of H₂ in amorphous polyethylene system: H₂ diffusion in various PE matrices and bubbling during rapid depressurization

Jiawei Zhao ^a, Xingguo Wang ^a, Qingquan Yang ^a, Hua Yin ^a, Bo Zhao ^b, Shijun Zhang ^{a,*}, Changjiang Wu ^{a,**}

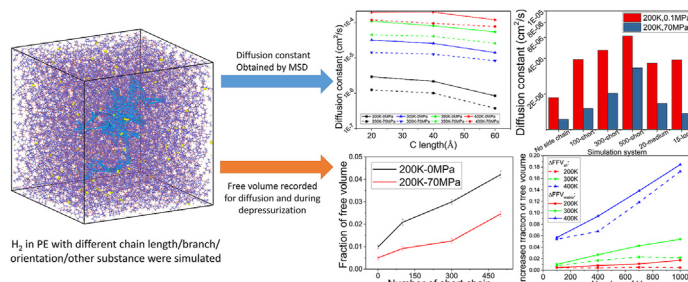
^a Beijing Research Institute of Chemical Industry, SINOPEC, Beijing 100013, People's Republic of China

^b Institute of Chemistry, China Special Equipment Inspection and Research Institute, Beijing 100029, People's Republic of China

HIGHLIGHTS

- H₂ behaviour in amorphous PE was simulated by molecular dynamic.
- PE branching and orientation affect H₂ diffusion in its amorphous region.
- 2D nanofiller can improve barrier property but need to be carefully processed.
- H₂ nanobubble observed during rapid depressurization simulation.

GRAPHICAL ABSTRACT



ARTICLE INFO

Article history:

Received 25 July 2022

Received in revised form

9 September 2022

Accepted 12 September 2022

Available online 5 October 2022

Keywords:

Hydrogen diffusion
Polyethylene
Molecular dynamics

ABSTRACT

Polyethylene (PE) is a candidate liner material for Type IV storage devices. In this case, all-atom molecular dynamics simulations are employed to study the properties of Polyethylene with the presence of H₂, including tensile properties, glass transition, diffusion in different PE and bubbling during rapid depressurization. The presence of H₂ deteriorates the polyethylene matrix's tensile performance and decreases the glass transition temperature. The branch, side chain and small molecules promote the diffusion of H₂ in the amorphous region by introducing more free volume below Tg. With a sufficient length, the length of polymer chain has minor effect on the diffusion of H₂. Graphene, as a 2D reinforcement, could decrease the diffusion of H₂ but suffers from poor interfacial bonding. Finally, H₂ bubble(s) formed from the over-saturated H₂ molecule and were observed in both the exclusive and free volume and stabilised at low pressure during rapid depressurization. According to the result obtained in this work, branchless HDPE is expected to give superior performance while the viscosity, which is important during processing, could

* Corresponding author.

** Corresponding author.

E-mail addresses: zhangsj.bjhy@sinopec.com (S. Zhang), wuchangjiang.bjhy@sinopec.com (C. Wu).

<https://doi.org/10.1016/j.ijhydene.2022.09.124>

0360-3199/© 2022 Hydrogen Energy Publications LLC. Published by Elsevier Ltd. All rights reserved.

be tailored by molecular weight. Processing technique leads to orientation is preferred, such as injection moulding.

© 2022 Hydrogen Energy Publications LLC. Published by Elsevier Ltd. All rights reserved.

Introduction

Hydrogen gas as an energy source is increasingly demanded because it is environmentally friendly and has no carbon emissions. Type IV hydrogen storage device, which is composed by a polymeric liner and carbon fibre composite shell, is an ideal choice for high-pressure hydrogen gas storage for its weight efficiency [1–5]. Polyethylene (PE) is a promising candidate material for the liner of type IV hydrogen storage devices [3,5,6]. The liner, which contains high-pressure hydrogen gas up to 70 MPa, 85 °C, is designed to minimize the dissipation of the hydrogen gas [1–3,6]. Despite several experimental works being successfully conducted [7–11], long equilibrium time and potential leakage under high pressure make experimental works time-consuming and dangerous. On the other hand, H₂ is one of the smallest gas molecules and has poor interaction with polyolefin polymers, which results in relatively high gas permeability [12,13]. The amorphous region of PE was commonly seen as the main route of the H₂ diffusion among the polymer matrix while the crystallised phase prohibited the H₂ diffusion with higher density and more compact structure [7,14–16]. Recent advance has revealed that the different type of PE, ranging from low density polyethylene (LDPE) to ultra-high molecular weight polyethylene (UHMWPE), may have different diffusion constant ranges from 1×10^{-5} to $1 \times 10^{-7} \text{ cm}^2/\text{s}$ [6,8,17,18]. However, the measure of the H₂ diffusion based on experimental are affected by several factors which can be hardly rule out. First of all, orientation, crystallinity and even gas solubility of the sample could be adjusted by not only chain structure but also processing parameters [19–22]. Also, the crystallisation of PE could be finished in minutes, which make the effect of the crystallinity could not be ruled out in the experimental work [20,21]. Also, the experimental results are affected by its procedure [11,17,18]. The effect of the molecular structure of the PE on the diffusion of H₂, especially the diffusion in the amorphous region with different branches/side chain was still not revealed.

Blister damage of the polymer matrix during the rapid depressurization of hydrogen gas is also a hot topic [6,18,23–28]. During an event of rapid depressurization, H₂ molecules do not have enough time to diffuse out of the polymer matrix. Experimental works evident that there are two states of H₂ that may be presented in a polymer matrix, which are isolated H₂ molecular and H₂ microbubbles [29,30]. The isolated H₂ molecules are expected to be fully/over saturated under high pressure and aggregated during rapid decompression [23,28]. The H₂ microbubbles are expected to expand during rapid decompression with an anisotropic fashion [24,27]. Research conducted by transmission electron microscopy concluded that the blister fracture initiated from bubbles with a size of several nanometres [31]. Numerical

studies, such as finite element analysis and analytical modelling, are also carried out to investigate the cavitation during rapid depressurization [6,23,24,26]. However, the initial stage of blister fracture, especially the aggregation of separate H₂ molecules during rapid depressurization, is still not clear. A previous study revealed that the cracking formation during the blister is related to the tensile properties [24]. As the H₂ molecular is expected to be concentrated in the amorphous region, the tensile properties and its glass transition temperature (T_g) of amorphous polyethylene with the presence of H₂ molecular is worth to be investigated.

The molecular dynamics (MD) simulation could be a useful tool to study the diffusion of gas molecules in polymer matrixes. By utilizing the Einstein relationship [32] and calculating the mean square displacement of the centre of mass of gas molecular in particular matrix, various diffusion constant was successfully calculated with all-atom molecular dynamics simulation, such as H₂ [33,34], O₂ [35–39], N₂ [35,36,38], CO₂ [33,37,40,41], Noble gas [33,40] in different matrix, such as polyolefin [40,42], polystyrene [34], rubber [35,38,43], PDMS [42], ionic liquid [33], Modified polystyrene [36], various polyester [37,41,44], PAN [45], Nylon [45,46], PEO [45] and their copolymer/composite. Despite many simulation works focused on gas diffusion in different polymer matrixes, the effect of polyolefin chain structure on H₂ diffusion has still not been investigated. In this work, classical all-atom molecular dynamics simulation is employed to investigate the effect of structure of PE on H₂ diffusion in amorphous region. The PE systems were constructed with different chain length, chain structure and orientation so that the influence on the H₂ diffusion constant were discussed and calculated without other interference. Also, to better understand the blister damage during rapid decompression, the tensile property and glass transition of amorphous PE system with various concentrations of H₂ were investigated by MD. Finally, the clustering of H₂ molecules within the amorphous PE/H₂ system during the rapid depressurization was revealed by MD with the assumption that the diffusion could be omitted.

Simulation details

Force field and structure generation

All simulations were conducted on Large-scale Atomic/Molecular Massively Parallel Simulator (LAMMPS) [47]. AIREBO-Morse potential, which is a special fitted empirical potential for hydrocarbon systems under pressure and consistent with the ab-initio calculation, was used in all simulations in this work [48]. The temperature and pressure were controlled by Nose-Hoover thermostat and barostat [49,50]. Considering the massive difference between the mobility of polymer atoms and H₂ atoms, the temperature and pressure control, if being

applied on a polymer/H₂ hybrid system, were only applied to polymer atoms to avoid overheating of the H₂ molecular as reported previously [40]. Two types of systems were used in this work, which are the finite chain models and the infinite chain models. All the finite chain models were initially created by an in-house code with low density to avoid any close contact following the protocol stated below. The generated systems were then compacted in an isothermal-isobaric ensemble with 300 K, 100 MPa for 200 ps to a reasonable density. After the structures were compacted, all systems were relaxed in desired temperature and pressure for 300 ps and then conducted the required simulation. All visualisation and part of the data analysis were conducted by OVITO [51].

To generate the finite length chain models, a randomized self-avoid walk method has schemed with restrictions during structure generation, which is given below:

$$\begin{cases} DP_{main} + \sum_{i=0}^{n_{sc}} DP_{sc,i}, i = DP_{total} \\ DP_{main} > DP_{main,min} \\ DP_{sc,i} > DP_{sc,min} \end{cases} \quad (1)$$

Where DP_{total} is the total degree of polymerization, DP_{main} is the degree of polymerization of main chain, DP_{sc,i} is the degree of polymerization of side chain *i*, n_{sc} is the number of the side chain. DP_{main,min} and DP_{sc,min} is the minimum value of the degree of polymerization of main chain and side chain. Note that the DP_{main,min} + $\sum_{i=0}^{n_{sc}} DP_{sc,min}$ is lower than DP_{total} in most cases and the rest of the DP will be randomly distributed to main chain and each side chain. The position of the side chain is completely random distributed on the main chain with a restriction of any side chain cannot be allocated near another side chain within 4 DP. To perform the simulation close to the real scenario, the total degree of polymerization of the involved PE chain needs to be high enough to represent the real scenario. In this work, the standard PE chain length was set as a total degree of polymerization (DP_{total}) equal to 2000, which is equivalent to molecular weight of 56 kg/mol and close to the real polyethylene pallets in service. If DP_{total} = 2000, 4 chains were used in the simulation system to make sure the system has sufficient volume to safely neglect the potential error introduced by the periodic boundary condition. To simulate the effect of chain length on H₂ diffusion constant, 1 DP_{total} = 8000 chain, 2 DP_{total} = 4000 chains, 8 DP_{total} = 1000 chains and 16 DP_{total} = 500 chains were simulated. Those systems with different DP have a similar volume with 4 DP_{total} = 2000 chains system. To investigate the effect of branches/side chain on H₂ diffusion constant, systems contain 100 short branches (100-short)/300 short branches (300-short)/500 short branches (500-short)/20 median side chains (20-median) and 15 long side chains (15-long) were simulated. For Those systems contains branches, the DP_{total} were set to 2000. The short branches have an average DP less than 2 with no single branches are longer than 4 carbon atoms. The medium side chains have an average DP of 27.61 and the long side chains have an average DP of 65.9. Note that with the introduction of the branches/side chain, the length of the main chain is shortened to keep the DP_{total} constant. To investigate the effect of plasticisers, 10-mer linear short PE

Table 1 – The finite chain model generated in this work.

N (chains)	DP _{total}	n _{sc}	DP _{main,min}	DP _{sc,min}	Other sub.
4	2000	0	N/A	N/A	N/A
1	8000	0	N/A	N/A	N/A
2	4000	0	N/A	N/A	N/A
8	1000	0	N/A	N/A	N/A
16	500	0	N/A	N/A	N/A
4	2000	100	1800	0	N/A
4	2000	300	1500	0	N/A
4	2000	500	1300	0	N/A
4	2000	20	1300	20	N/A
4	2000	15	500	20	N/A
4	2000	100	N/A	N/A	46xC ₂₀ H ₄₂
4	2000	100	N/A	N/A	89xC ₂₀ H ₄₂
4	2000	100	N/A	N/A	1xGraphene

chains, which has a formulation of C₂₀H₄₂, were added in DP_{total} = 2000, 4 branchless chains system as the plasticisers. 46 and 89C₂₀H₄₂ molecule were added in the system, yield a weight percent of plasticizer at 5.47 wt% and 10.07 wt% respectively. To investigate the effect of potential reinforcement of 2D nano-fillers, a graphene layer was added to represent 2D nanofillers in DP_{total} = 2000, 4 branchless chains system. The graphene layer was constituted with 2376 carbon atoms and yield a weight percent of graphene at 11.28w.t%. The graphene layer fits the length of the X and Y axis and bonded to itself via periodic boundary condition, which means it is infinite long in those 2 axes. The DP_{total}, n_{sc}, DP_{main,min}, DP_{sc,min} and other substance used in each finite chain length model were listed in Table 1.

A series of orientated PE structures were generated with infinite chain length. For each system, a 11x16x31 supercell of PE crystal was firstly generated, yielding 20,212 CH₂ units. All PE chains are orientated along with the Z axis. The crystallised PE was then heated up to 600 K to fully melt the crystal structure for 250 ps. After the crystallised structure is fully melted down, the Z axis was pulled to 20/40/60 Å respectively and the other axes were controlled by an isothermal-isobaric ensemble at 400 K, 70 MPa for 200 ps. Then, the systems were fully relaxed in the desired temperature and pressure for 200 ps with the length of Z axis fixed. Note that the fully melt down system yield a C length of ~19.17 Å at 400 K and the fully crystallised system yield a C length of ~78.71 Å. Those two values could be seen as the orientated free state and fully orientated state respectively and one could use the Z-axis length to represent the degree of orientation. Configuration of a branchless system with DP_{total} = 2000 and orientated system with Z axis equals 60 Å were given in Fig. 1 to show the size of the corresponding system. The trajectories of 5 random chosen H₂ molecules were also shown in Fig. 1 as grey solid lines to represent the difference between diffusion patterns of the system with and without orientation. The trajectories shown in Fig. 1 were generated by the simulation at 300 K, 70 MPa.

Diffusion constant calculation

Considering the working condition of the liner, the diffusion constant simulations were conducted under temperature = 200, 300, 350, 400 K and pressure = 0 MPa, 70 MPa. The total

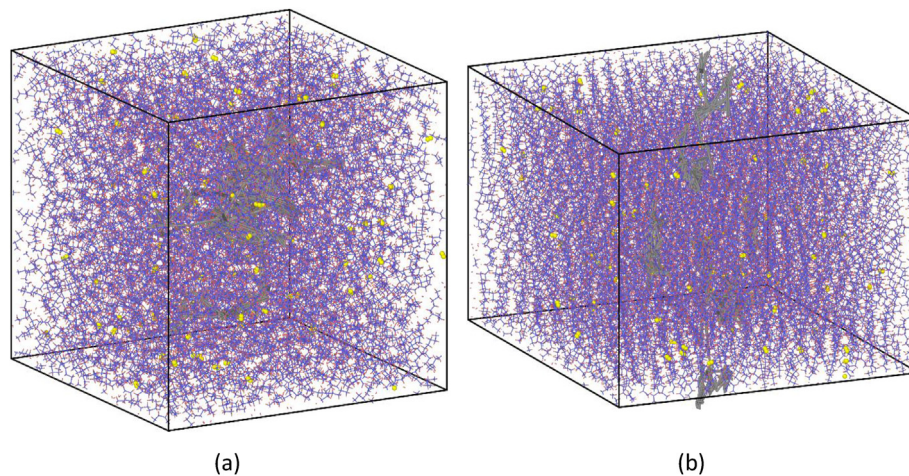


Fig. 1 – Configuration of a branchless system(a) and orientated system(b), The DP of the branchless system is 2000. The Z axis length is 60 Å for the orientated system. The yellow atoms represent atoms in H_2 molecules. The polymer parts were present with bond only, as the blue ends represent carbon atoms and the red ends represent hydrogen atoms. The grey solid lines are the selected H_2 diffusion trajectories. (For interpretation of the references to colour in this figure legend, the reader is referred to the Web version of this article.)

time length of the simulations were 1 ns. During each simulation, 100 H_2 molecules were added into the system to calculate the diffusion constant. The mean square displacements (MSD) of the centre of mass for each H_2 molecule were recorded during the simulation and the diffusion constant of H_2 molecule could be calculated by the Einstein relationship given in equation (2) by using the latter half of the MSD obtained from the simulation [34,39,41,43,45,52–55].

$$D = \lim_{t \rightarrow \infty} \frac{1}{6N} \left(\frac{d \sum msd(t)}{dt} \right) \quad (2)$$

To further explain the difference of molecular structure between simulated PE systems, the fraction of free volume (FFV) was calculated by OVITO using a 3 Å probe for several systems. The cutoff radius is chosen to be 3 Å as it is the equilibrium distance between H_2 molecule in gas phase determined by a previous study [56].

Tensile properties and glass transition temperature

To investigate the effect of H_2 content on the tensile properties and glass transition, 4 branchless, $DP_{\text{total}} = 2000$ PE chains with were simulated with 0, 100, 200, 300, 400, 500, 600, 700, 800, 900 and 1000 H_2 molecules. Those systems were firstly initialized and elongated with an engineering strain rate = 10^9 s^{-1} to a 25% strain to calculate the elastic modulus and yield stress. The elastic modulus under $T = 200 \text{ K}$ and $P = 0 \text{ MPa}$ were calculated. The yield stress was recorded as the maximum stress achieved during each simulation. To calculate the glass transition temperature (T_g), 4 branchless, $DP_{\text{total}} = 2000$ PE chains with 0, 500, 1000 H_2 molecules were firstly initialized and held at 400 K, 0 MPa. Then those simulation systems were cooled from 400 K to 200 K in 10 ns under 0 MPa, which yields a cooling rate of $2.0 \times 10^8 \text{ K/s}$ and the density was recorded. As T_g could be defined as the temperature which $\frac{d\rho}{dT}$ changed, two linear regressions were conducted on the 200–250 K and

300–350 K and the T_g was recognised as the temperature of the interception point between two linear regressions.

Bubbling during rapid depressurization

To simulate the blister damage during rapid depressurization, 4 branchless, $DP_{\text{total}} = 2000$ PE chains system containing 100, 400, 700, 1000 H_2 molecules were firstly initialized and held at 200 K-70 MPa, 300 K-70 MPa and 400 K-70 MPa for 300 ps and then the pressure was suddenly dropped to 0 MPa and simulated for 500 ps to observe the bubble growth. During those simulations, H_2 molecules were assumed that cannot escape the polymer matrix from polymer/gas interphase due to insufficient diffusion time. The accurately calculation of blister damage with different depressurization rate requires a significant larger system to contain explicit polymer/gas interphases. Such large system is hard to be calculated within this methodology because of the computational resources needed and more suitable for united atom/coarse grain MD calculation. To track the difference between systems, two fractions of free volume (FFV) were calculated for each system with a 3 Å cutoff radius by OVITO, similar to the process given in the previous diffusion constant calculation section. The first FFV considered all atoms in the system, which is labelled as FFV_{all} . The second FFV considered only polymer matrix in the system, which is labelled as FFV_{matrix} . The H_2 bubble content than could be obtained by $FFV_{\text{matrix}} - FFV_{\text{all}}$. The increment of FFV_{all} and FFV_{matrix} during depressurization were calculated for each system to evaluate their break down, labelled as ΔFFV_{all} and $\Delta FFV_{\text{matrix}}$ respectively. The ΔFFV_{all} and $\Delta FFV_{\text{matrix}}$ are calculated by average the FFV for the latter half of the pressure drop simulation and minus the corresponding value at the beginning of the simulation.

To further investigated the depressurization of the PE/ H_2 system, 4 branchless PE chains with $DP_{\text{total}} = 2000$ containing 1000 H_2 were subjected to a 10 ns simulation where the

pressure was decedent from 70.1 MPa to 0.1 MPa at 400 K. To focus on H₂ agglomerated region, the ΔFFV_{all} and ΔFFV_{matrix} were calculated with a 6 Å cutoff radius by OVITO.

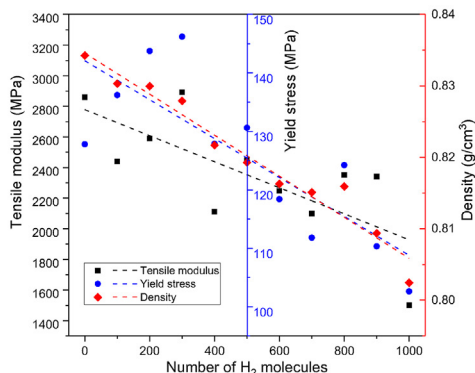
Results and discussion

The effect of H₂ molecules in tensile properties and glass transition temperature

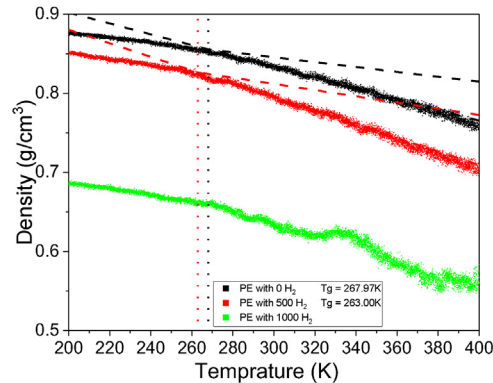
The tensile properties, including yield stress and tensile modulus are illustrated in Fig. 2(a) with its density at beginning of elongation. The density turns to have a clear decreased trend with the increment of H₂ content. Despite there is some level of noise, a decreased trend could also be found of the tensile modulus with the increment of H₂ content. An increment trend of yield stress could be found while the amount of H₂ molecules is less than 300, then dropped after the amount of H₂ molecules became more. The result could be explained by the poor interaction between H₂ molecules and polyolefin chains [12]. Furthermore, as a gas molecule, H₂ molecules are not expected to have any outstanding mechanical performance in bulk. In

this case, H₂ molecules are not expected to mechanically reinforce the matrix. We speculated that the effect of H₂ molecules on the tensile properties is similar to voids as the mobility of H₂ and the poor interaction between PE and H₂. It is worth to mention that the strain rates used in simulations are high compared to the experimental work, which is currently restricted by the computational cost. The high strain rate may be hindered any relaxation and increase the modulus.

The calculated Tg for PE containing 0/500H₂ molecules is 268.0 K and 263.0 K respectively, as shown in Fig. 2(b). For the system of PE/1000H₂, the density-temperature curve is similar to the PE/500H₂ system. However, the Tg for the PE/1000H₂ system cannot be obtained due to the abnormal trends in the region of T = 300 K to T = 350 K. The abnormal of the trend is suspected to be related to the phase separation in PE/1000H₂ system, as shown in Fig. 2(e). Compared with Fig. 2(c) and (d), The configuration shown in Fig. 2(e) has a H₂ enriched area. The simulation overestimates the Tg compared to the experimental value as the cooling rate is high but close to several computed Tg [57–59]. The simulation indicates that the presence of the H₂ lower the Tg of the system. Similar results were also observed in previous experimental research [11,60].



(a)



(b)

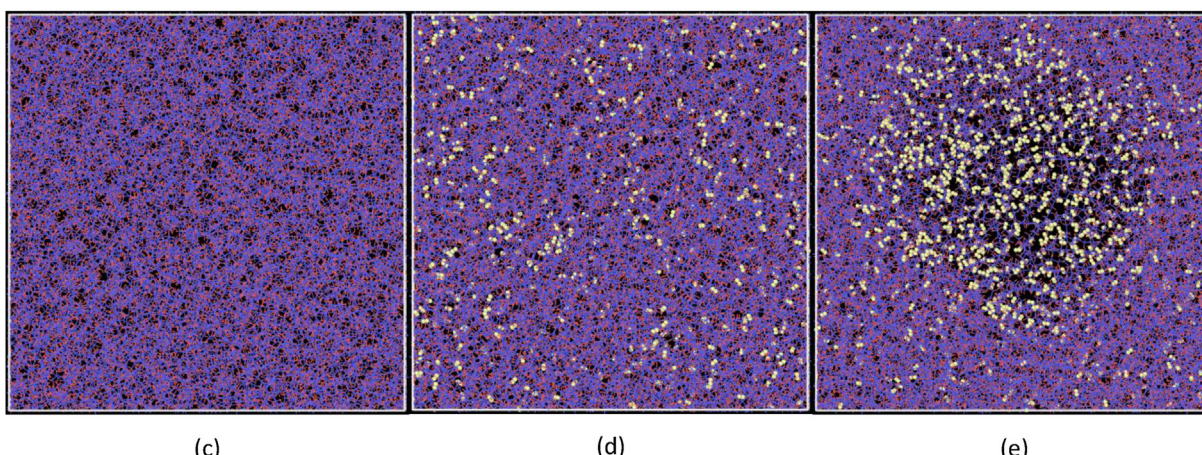


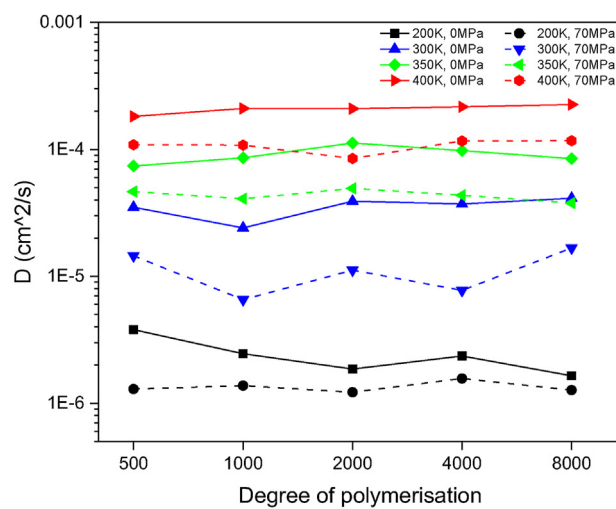
Fig. 2 – The effect of H₂ molecules content on tensile properties and density with T = 200 K and P = 0 MPa(a), density against temperature for branchless PE with 0/500/1000H₂ molecules (b) and the initial configuration of Tg simulation of PE/0H₂(c), PE/500H₂(d), PE/1000H₂(e). The yellow atoms represent atoms in H₂ molecules. The polymer parts were present with bond only, as the blue ends represent carbon atoms and the red ends represent hydrogen atoms. (For interpretation of the references to colour in this figure legend, the reader is referred to the Web version of this article.)

The effect of polymer structure on the diffusion constant: degree of polymerization, side chain and orientation

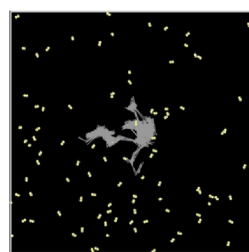
The diffusion constant of H₂ in polyethylene with different DP is calculated and given in Fig. 3(a). From Fig. 3(a), we could not find any conclusive evidence that the diffusion constant is significantly affected by the degree of polymerization. Some research concluded a negative correlation between gas diffusion rate and DP [34,61]. However, given the fact that the chain length in this research is longer than most of the research in this area, the number of end groups, which is proportional to DP⁻¹, is significantly lower. On the other hand, there are some works showing that the diffusion rate of gas is less relevant with DP from both experimental and simulation works [17,62]. [40] During the experimental work, the diffusion constant of PE sample is affected by not only the molecular structure, but also the processing condition. The processing condition could affect the orientation and crystallisation within the sample and results in different diffusion constant. Despite the

diffusion constant obtained by previous experimental work may be affected by other factors, the result obtained in this work and the previous obtained experimental result indicates that the diffusion constant show less correlation with the degree of polymer if the chain is long enough [17,62].

The diffusion path of 5 random selected H₂ molecules in 200 K, 0 MPa and 400 K, 0 MPa were given in Fig. 3(b) and (c). In Fig. 3(b), a clear “defect jump” patent could be observed. At lower temperature, the result indicates that the H₂ molecules were mainly randomly moving in a free volume region and jump to a proximity free volume region at times, while the distribution of the free volume is relatively stable [34]. In Fig. 3(c), as the temperature increased, the trajectories become significantly widely dispersed, which indicates the diffusion path of each H₂ molecule was significantly longer compared to the low-temperature scenario. Also, the patent of the H₂ diffusion is less regular which indicated the distribution of the free volume may become relatively unstable and redistribution of free volume may occur as the polymer matrix is in a



(a)



(b)



(c)

Fig. 3 – The relationship between DP and diffusion constant(a) and the diffusion path of H₂ in DP2000 PE in 200 K(b) and 400 K(c). Note that the simulation system, which presented by the white box in (b) and (c) has roughly the same boundary length (76.00 Å for (b) and 79.15 Å for (c)).

rubbery state [34]. In this case, the H₂ molecules may be “pushed” during free volume redistribution and the relation between diffusion constant and MSD may deviate from the Einstein relation [40].

Fig. 4 shows the effect of short branches/side chains structure on the H₂ diffusion constant in the PE amorphous phase. Considering PE is a polymer that has one of the highest degrees of crystallisation in reality, the amorphous phase is more constrained and rigid as it is in the proximity of the crystal phase compared to a completely free amorphous phase. In this case, it is reasonable to use an amorphous phase at lower temperature to represent a more rigid amorphous phase. The 200 K, which are the low-temperature systems in this research, were used to represent the actual rigid

amorphous phase and the H₂ diffusion constant of the related systems were shown in Fig. 4(a). One could recognize from Fig. 4(a) that the branchless PE has the lowest diffusion constant. From the comparison with side branchless systems (100-short, 300-short and 500-short) one could summarise that as the number of short branches increases, the diffusion constant increased at a lower temperature. The result obtained in the simulation coincides the experimental outcome presented in Ref. [17]. The result could be explained by the stereo effect straight forward as the irregular short branches hindered a compact configuration between chains. On the other hand, the longer side chains, represent by systems containing 15-long and 20-medium side chains, seem to show less difference on the H₂ diffusion constant with the length of

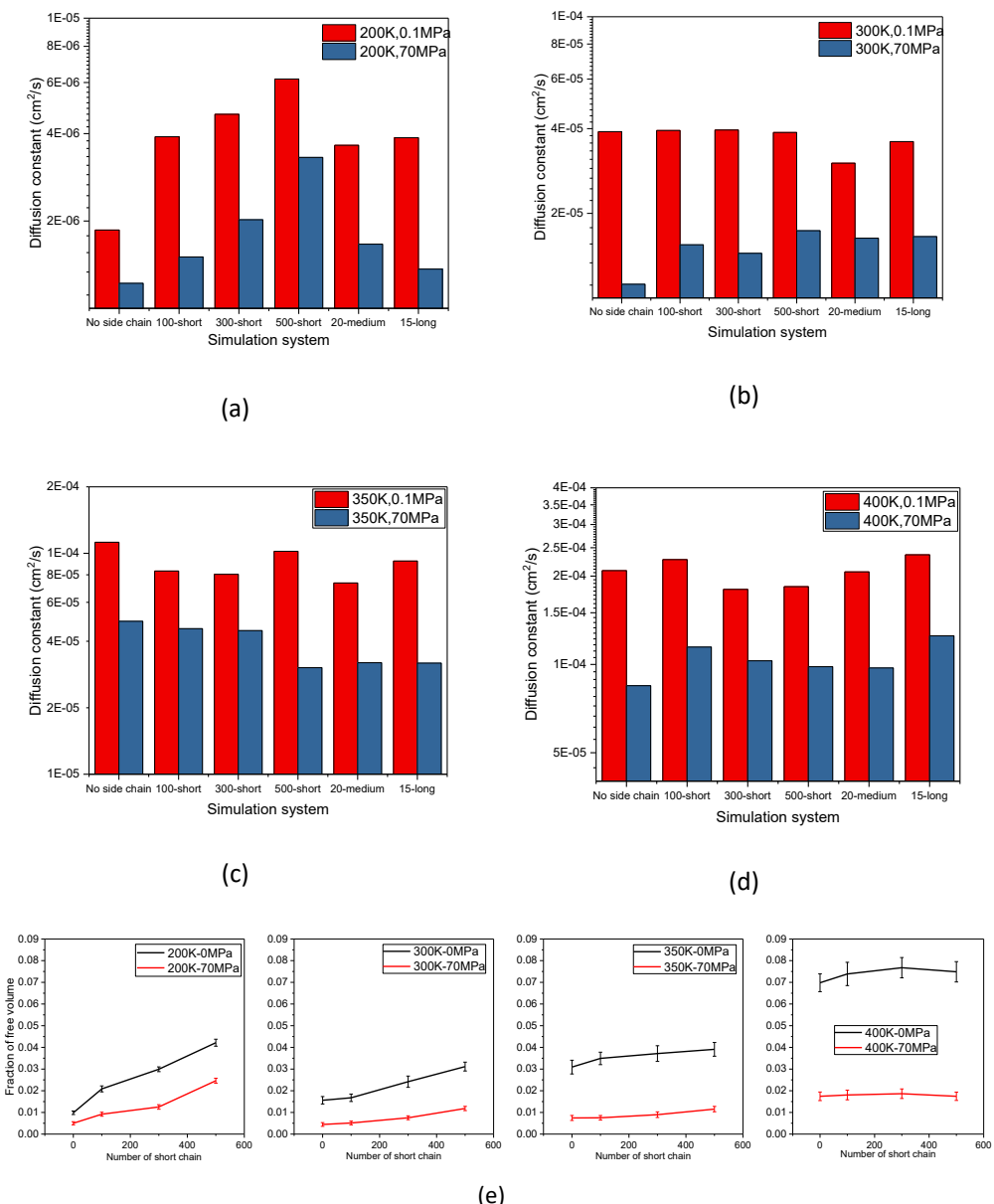


Fig. 4 – The H₂ diffusion constant in PE with different branch/side chain systems at 200 K (a), 300 K (b), 350 K (c), 400 K (d) and the FFV against the short branch in different temperature (e).

the side chain significantly altered. The effect of the branch/side chain is the same but less significant under high pressure as the structure become overall more compact compared to the pressure-free systems. From Fig. 4(b), Simulations conducted at 300 K, 70 MPa follows the trends obtained in 200 K. However, simulations conducted at 300 K, 0 MPa did not follow the same trend and present that the diffusion constant is less relevant to the number of side branches. The differences in trend could be explained by the glass transition of PE matrix at 268.0 K as stated above without pressure. When pressure is applied, the T_g is expected to increase thus the 300 K-70 MPa system may also stay in glassy state.

Fig. 4(c) and (d) present the H₂ diffusion constant in PE with different chain structures in 350 K and 400 K. The 350 K and 400 K systems represented an overheated and melted PE system as the liner material could withstand a temperature up to 85 °C which may cause a partial breakdown of small crystal regions at the very edge of the liner. The result indicates that the H₂ diffusion constant in such temperature does not show a clear relationship with the presence of branches and side chain in the melt stage, which is similar to the trend present among simulations conducted at 300 K, 0 MPa. As the motion of the polymer chain become significant above T_g, the

redistribution of free volume promotes the H₂ diffusion and weakens the influence of the presence of branch/side chain.

Fig. 4(e) shows the fraction of free volume (FFV) against the change of the number of the short branches, an increasing trend could find at 200, 300 and 350 K. The FFV increment against the presence of the short branches became less significant with temperature increased. At 400 K, the FFV did not show a significant dependency on the Number of short chains. The diffusion of H₂ changed accordingly, which supports the explanation of the trend of the H₂ diffusion constant. It is worth mentioning that the standard error is also increased with the temperature increase, with the expectation of from the 200 K, 70 MPa system to 300 K, 70 MPa system, which may indicate the amorphous region becomes less stable in higher temperature and support the free volume may redistribute. This will lead to deviation from the Einstein relationship as the motion of the polymer chain become significant and cannot be ignored [40].

Fig. 5 presents the relationship between the PE chain orientation and diffusion constant of the H₂ molecule, with the Z-axis length to represent the degree of orientation. From Fig. 5(a), the results indicate that the chain orientation decreased the diffusion constant of H₂ in the system. This

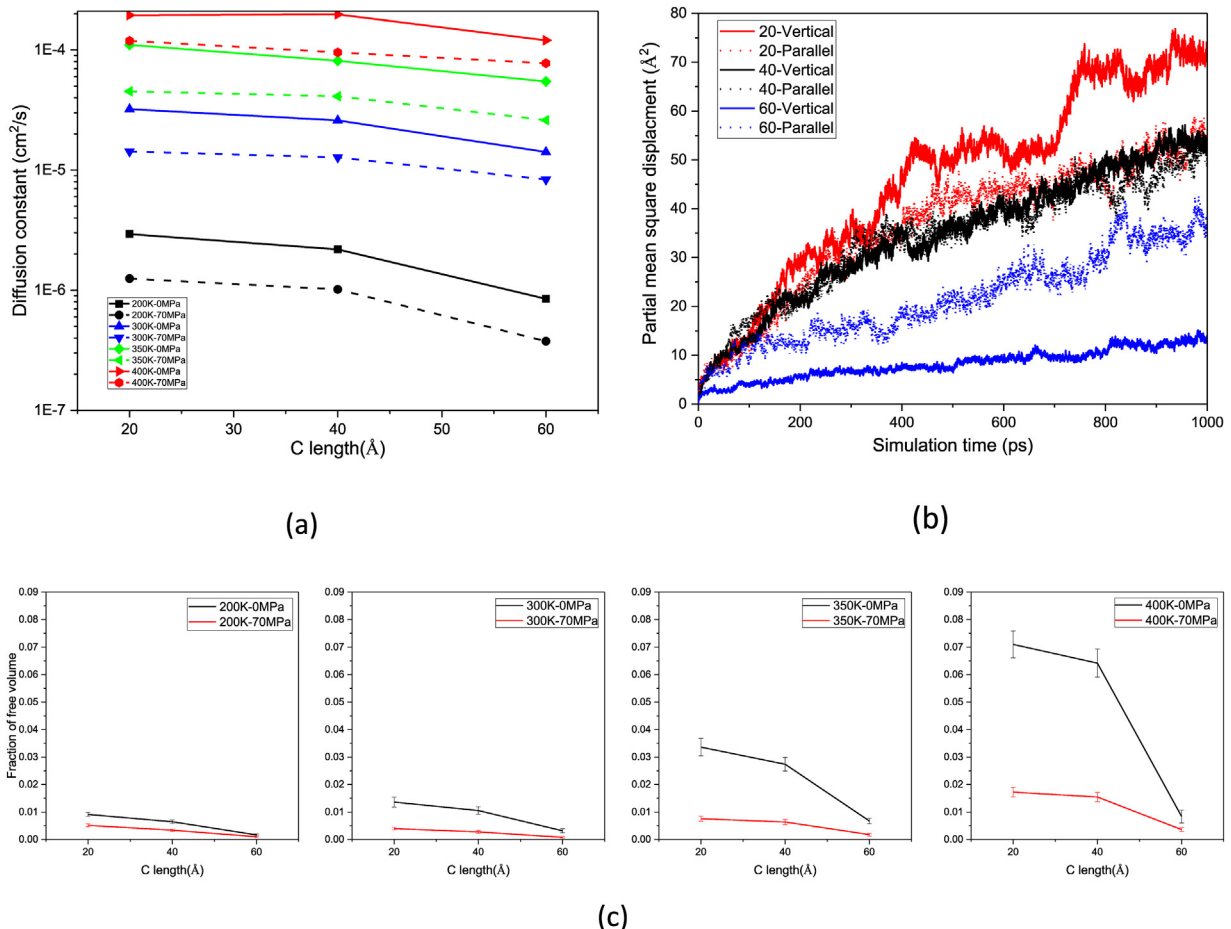
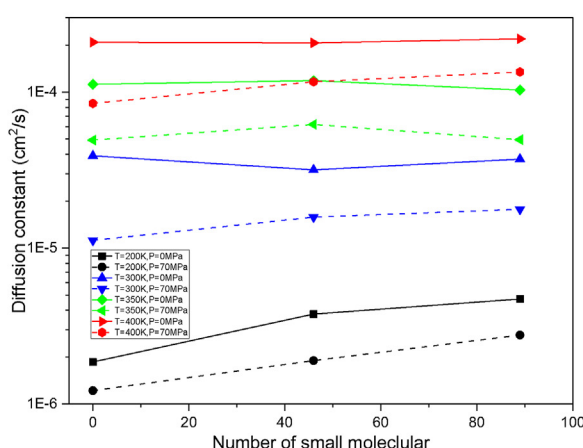


Fig. 5 – The effect of chain orientation on H₂ diffusion constant (a), the partial MSD on the vertical and horizontal direction to the chain orientation at 200 K-0 MPa (b) and the FFV against different orientation degrees at different temperatures and pressure (c).

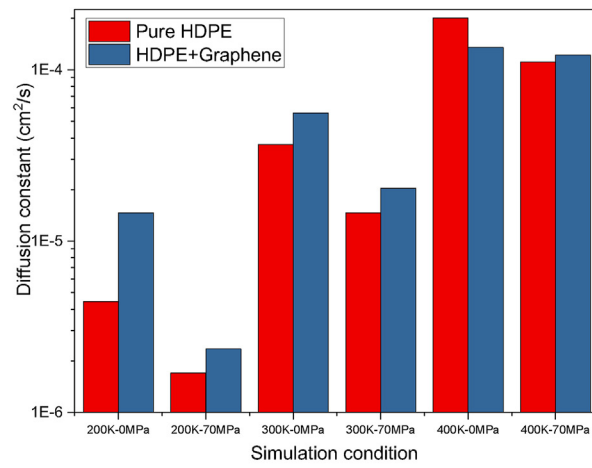
could be explained as the presence of chain orientation systems have a denser compact compared to the orientation-free system, which is supported by the FFV statics given in Fig. 5(c).

As stated above, the amorphous phase will be constrained by crystal phase and the disorientation of PE chains will be hindered in such case. The 200 K-0 MPa system was selected for detailed analysis, as shown in Fig. 5(b). The partial MSDs, which are parallel and vertical to the orientation direction against simulation time, are given by $\frac{\Delta x(t)^2 + \Delta y(t)^2}{2}$ and $\Delta z(t)^2$ respectively and plotted in Fig. 5(b). In the least orientated system, one could conclude that the H₂ molecule diffused more rapidly in the vertical direction of chain orientation, rather than in the parallel direction of chain orientation. However, this difference may be caused by the periodic boundary condition as the simulation system is highly skewed at a size of 179 Å × 159 Å × 20 Å. The short Z axis granted a defect is within 20 Å and may self-interacted, promoting the H₂ molecular to diffuse through the vertical direction by “defect jump” mechanism. The other two systems, which had a size of 125 Å × 110 Å × 40 Å and 94 Å × 83 Å × 60 Å, is more regularly compared to the 20 Å system. Free volume in those two systems can be separated far enough to prevent self-

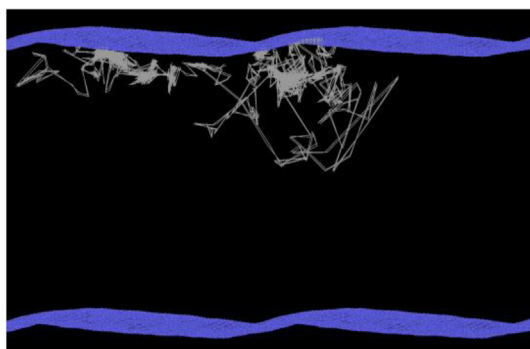
interacting. In this case, a similar degree of diffusivity could be found in both the parallel and vertical directions of the 40 Å system, which is also close to the diffusivity at the 20 Å system in the parallel direction. For the most orientated system, one could conclude that the diffusion of H₂ in both directions was decreased. The decrement is more significant in the vertical direction of the chain orientation. The trajectories of the H₂ molecule in the orientated system, as shown in Fig. 1(b), support the above analysis as all of the trajectories of H₂ diffusion are partially orientated with Z axis. As the chain is highly orientated, the orientation of the chemical bonds could explain the heterogeneous decrement of diffusibility, which also leads to the drop of the FFV illustrated in Fig. 5(c). As a bonded pair of atoms has a smaller gap compared to a non-bonded pair, the bonded pair of atoms could intercept H₂ molecules more effectively. With the alignment of bonded C-C pairs with one direction, the H₂ diffusion against orientation was decreased, which causes the more significant decrement of H₂ diffusion constant in the vertical direction of chain orientation. In this case, a sufficient degree of chain orientation could be effective against the diffusion of H₂ molecules particularly if the orientation is vertical to the pressure drop direction. The result indicated that processing



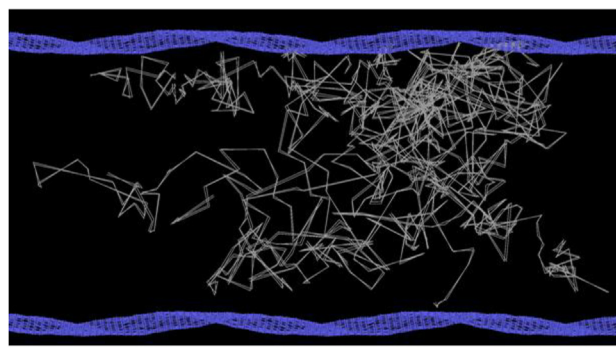
(a)



(b)



(c)



(d)

Fig. 6 – The effect of small molecules(a) and a continuous graphene layer(b) on the H₂ diffusion. The trajectories of 10 randomly selected H₂ molecules in graphene reinforced system of 200 K and 400 K are shown in (c) and (d), the distance between the illustrated graphene layer is similar in (c) (84.98 Å) and (d) (86.80 Å).

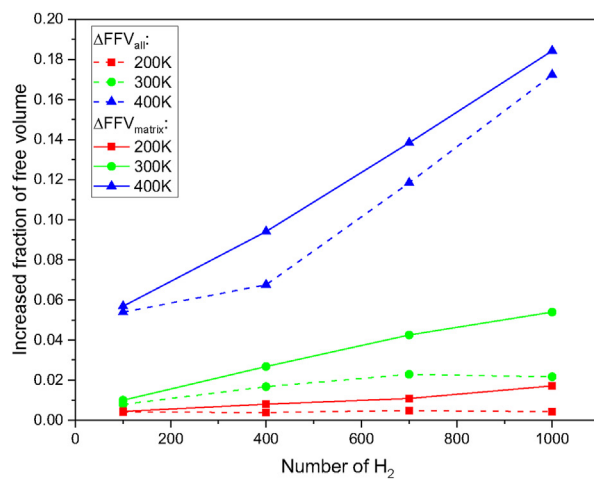
techniques, which could introduce chain orientation, are beneficial to the barrier properties of the PE matrix, such as injection moulding.

The effect of additive and reinforcement on H₂ diffusion in polyethylene

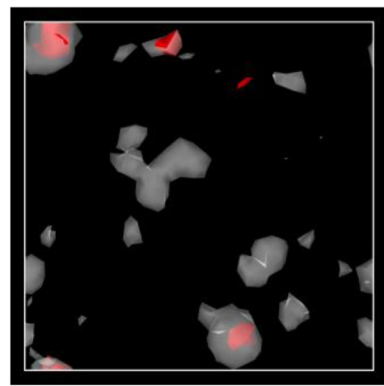
The H₂ diffusion constant of the systems that contain small molecules (represent as C₂₀H₄₂ as stated above) is given in Fig. 6(a). One could conclude that the H₂ diffusion constant increased with the presence of the small molecule in T = 300 K, P = 70 MPa, T = 200 K, P = 0 MPa and T = 200 K, P = 70 MPa systems, which share a similar trend with previous research on Nylon 11 [11,63]. The other systems, similar to the effect of the side chain, did not show a clear relationship as they go above the Tg of PE. The result could be explained as the plasticizing effect with the presence of the small molecule. The small molecule, acts as a plasticizer, promotes chain

mobility by introducing more free volume into the system below Tg. Thus, the H₂ diffusion constant is increased with the presence of small molecules.

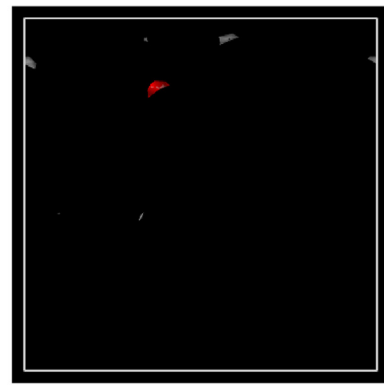
The comparison of the H₂ Diffusion constant of PE system and graphene/PE composite system was shown in Fig. 6 (b), and the trajectories of 10H₂ molecules were given in Fig. 6 (c) and Fig. 6 (d) of 200 K and 400 K, 0 MPa respectively. As shown in the graph, with the presence of the graphene layer, the H₂ diffusion constant is increased in lower temperatures and decreased in higher temperatures. From Fig. 6 (c), one could conclude that the diffusion of H₂ molecules is promoted at the interphase of graphene and PE. This could be further explained as the interaction between PE and graphene is relatively poor as only van der Waals force is expected [64,65]. In the meantime, the diffusion constant dropped with the presence of the graphene while the temperature at 400 K and the trajectories of H₂ were intercepted by graphene as present in Fig. 6(d). As the temperature increase, the mobility of the



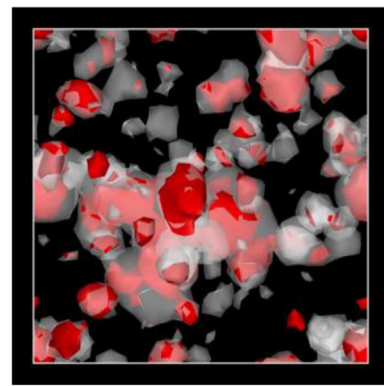
(a)



(c)



(b)



(d)

Fig. 7 – The ΔFFV_{matrix} (solid line) and ΔFFV_{all} (dash line) with respect to the H₂ content in systems with a probe size = 3 Å (a), and the FFV distribution in simulation cell of 1000H₂ system in 200 K (b), 300 K (c) and 400 K (d) with a probe size = 3 Å. The part in red corresponds to the ΔFFV_{all} and the part in white corresponds to the ΔFFV_{matrix} . (For interpretation of the references to colour in this figure legend, the reader is referred to the Web version of this article.)

polymer is promoted as the polymer matrix went through glass transition. However, the graphene layer may constrain the nearby polymer chains and intercept any H₂ molecular trying to pass it. In this case, we speculated that the free volume redistribution of the polymer chain near graphene was also restricted. Also, it is worth mentioning that this simulation was conducted without pressure drop. If a pressure drop exists, the H₂ molecules are expected to diffuse along with the pressure drop direction. This means that to maximize the effect of a layer filler, it should orientate against the pressure drop direction as being conducted in several experimental works [66–68].

Bubbling during rapid depressurization

Both the ΔFFV_{matrix} and the ΔFFV_{all} for DP = 2000, 4 branchless chains with 100, 400, 700 and 1000H₂ molecular systems were present in Fig. 7(a). The branchless systems are chosen because they have the lowest diffusion constant overall. The result indicates how the H₂ clustered during the depressurization, when diffusion is not sufficient. From the dash lines of Fig. 7(a), the ΔFFV_{all} for all systems have a positive correlation with the H₂ concentration. The result could be explained by more voids formed during depressurization as the H₂ gas is more sensitive to pressure. The solid lines, which represent ΔFFV_{matrix} , were also increased with H₂ content in all systems. The larger the difference between ΔFFV_{matrix} and the ΔFFV_{all} ($\Delta FFV_{all} - \Delta FFV_{matrix}$), the more the H₂ aggregated within the polymer. Considering there is no pre-aggregated H₂ microbubble in the simulation, the result supports that the dissociative H₂ may aggregate within the polymer matrix and to fill in the formed free volume during depressurization. One could conclude that, at 200 K and 300 K, with the increment of the

number of H₂ molecules, the $\Delta FFV_{all} - \Delta FFV_{matrix}$ during rapid depressurization is increased. At 400 K, the $\Delta FFV_{all} - \Delta FFV_{matrix}$ seems to peak at the number of H₂ molecules equal to 400. For the size distribution of the free volume of ΔFFV_{all} and ΔFFV_{matrix} , the free volume of the final structures of PE/1000H₂ system were selected to be visually inspected in Fig. 7(b)–(d) for temperature = 200, 300 and 400 K respectively. From Fig. 7(c)–(e). One could conclude that H₂ molecules are more volatile at a higher temperature and could form larger H₂ aggregation.

To further analyse the behaviour of the PE/H₂ system during rapid depressurization, a 10ns depressurization simulation was conducted on DP = 2000, 4 branchless PE with 1000H₂ system at 400 K. The bubble content was calculated by $\Delta FFV_{all} - \Delta FFV_{matrix}$ with a probe radius of 6 Å to detect larger H₂ bubbles. The bubble content and density were given in Fig. 8(a). Under the given condition, the gas bubble was first detected when the pressure dropped to ~35 MPa. However, the gas bubbles are not stable as they vanished and reappeared at ~24 MPa, ~16 MPa and ~8 MPa. At ~5 MPa, the bubble reappeared and begin to expand to form the final structure. As shown in Fig. 8(b)–(f), the visual inspected free volume indicates that the bubbles appeared at ~35 MPa, ~24 MPa, ~16 MPa and ~8 MPa were in different locations of the system, which supports that the bubbles generated under those pressure are not stable during simulation. The final configuration indicated that the gas bubble could have a size up to roughly 1–2 nm, which is observed in literature by a PVDF after high-pressure H₂ gas exposure [31]. The simulation support that an oversaturated polyethylene matrix with H₂ in high pressure could potentially form H₂ nanobubble during rapid depressurization if the depressurization process is too quick to allow sufficient diffusion to occur. As the in-situ x-ray tomography research was already

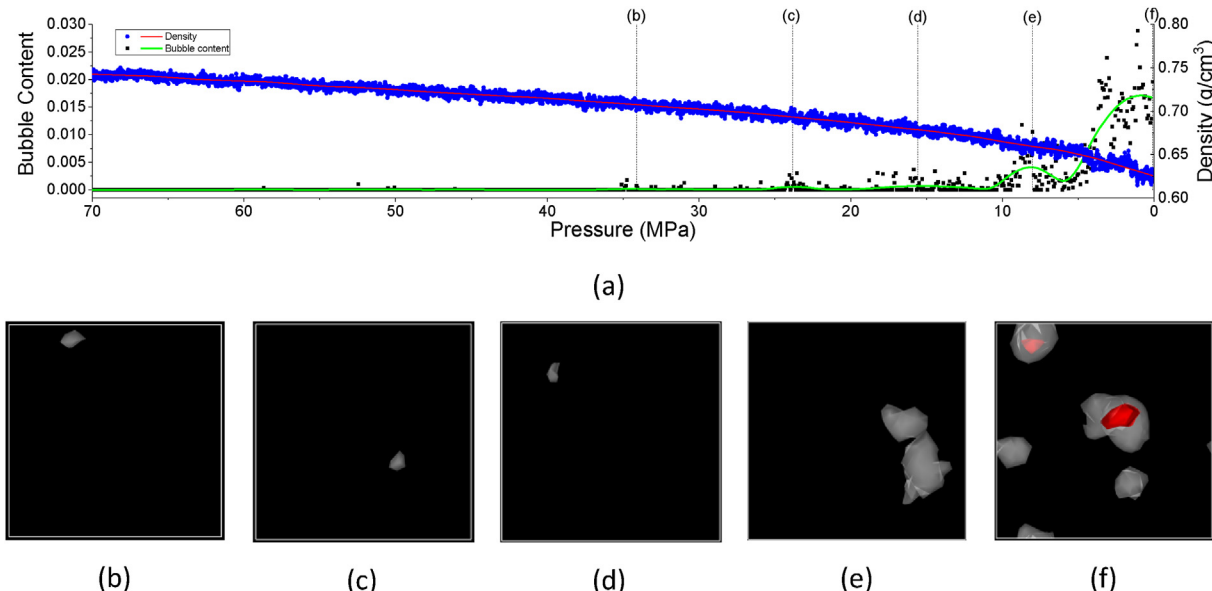


Fig. 8 – The bubble content with respect to the pressure of PE-1000H₂ system with probe size = 6 Å (a) and the H₂ bubble distribution at 34.12 MPa(b), 23.83 MPa(c), 15.57 MPa(d), 8.01 MPa(e) and 0.1 MPa(f). The part in red is the free volume and the part in white is the free volume with H₂ excluded. (For interpretation of the references to colour in this figure legend, the reader is referred to the Web version of this article.)

conducted, the author suggested that the in-situ small angle x-ray scattering (SAXS) and wide-angle x-ray diffraction (XRD) could be used to analysis the bubbling during the rapid depressurization, similar to the previous research conducted by Zhao et al. [27,69].

Conclusion

In this work, the tensile properties, glass transition, diffusion of H₂ and initial stage of the rapid depressurization were studied by molecular dynamics simulations. The result could be summarized as below:

- From the elongation simulation of the PE/H₂ system, one could conclude that the presence of the H₂ molecular jeopardizes the tensile properties of the amorphous part of polymer matrix and decrease the Tg of the system.
- It is evident that alongside the crystallinity, polymer chain structure impacts the diffusion constant in the amorphous region. Branches/side chains promote the H₂ diffusion in polyethylene under Tg by introducing more free volume. The more branches/side chains, the worse the barrier property. On the other hand, orientation, if carefully introduced against the pressure drop direction, could improve the barrier property. The diffusion constant is not significantly affected by chain length if the chain is long enough.
- The small molecules, act as a plasticizer, also increase the diffusion constant. For 2D reinforcement such as graphene, the preliminary simulation result indicates it could potentially be used as reinforcement to increase the barrier properties as it could intercept the H₂ diffusion against it. However, proper interfacial bonding needs to be achieved to prevent H₂ molecule diffusion through the interfacial region. If possible, the 2D reinforcement should be orientated against the pressure drop direction.
- The results of rapid depression simulation support the aggregation of H₂ molecules into nano-size bubbles in a polymer matrix if the depressurization is quick enough. A further MD simulation revealed that the bubbles may appear and vanish during pressure drop and may only be stable at very low pressure.
- Based on the result obtained in this work, branched PE are suggested to be avoid during material selection. Viscosity, which is important in a polymer processing prospective, is suggested to be tailored by molecular weight. Processing technique which could introduce orientation is recommended, such as injection moulding. Usage of small molecular are suggested to be avoid. Any potential reinforcing material is suggested to have a strong interfacial bonding and orientated against the pressure drop direction.

Declaration of competing interest

The authors declare that they have no known competing financial interests or personal relationships that could have appeared to influence the work reported in this paper.

Acknowledgement

This work is part of the hydrogen storage key project of SINOPEC Beijing Research Institute of Chemical Industry. The computational resources from SINOPEC Geophysical Research Institution were acknowledged and the authors would like to thank them for their support. J.Zhao appreciate the useful discussion with Dr. Jianye Liu, Dr. Wenxi Ji from Beijing Research Institute of Chemical Industry, Prof. Erqiang Chen from Peking University and Dr. Edrea Phua, Miss Yu Xiang from Loughborough University, UK. The authors appreciate the comments given by the reviewers during revision.

REFERENCES

- [1] Sapre S, Pareek K, Rohan R, Singh PK. Investigation of compressed hydrogen refueling process of 60 L type IV tank used in fuel cell vehicles. Energy Storage 2019;1:1–12. <https://doi.org/10.1002/est.2.91>.
- [2] Kim SC, Lee SH, Yoon KB. Thermal characteristics during hydrogen fueling process of type IV cylinder. Int J Hydrogen Energy 2010;35:6830–5. <https://doi.org/10.1016/j.ijhydene.2010.03.130>.
- [3] Balasooriya W, Clute C, Schrittesser B, Pinter G. A review on applicability, limitations, and improvements of polymeric materials in high-pressure hydrogen gas atmospheres. Polym Rev 2022;62:175–209. <https://doi.org/10.1080/15583724.2021.1897997>.
- [4] Heitsch M, Baraldi D, Moretto P. Numerical investigations on the fast filling of hydrogen tanks. Int J Hydrogen Energy 2011;36:2606–12. <https://doi.org/10.1016/j.ijhydene.2010.04.134>.
- [5] Wang X, Tian M, Chen X, Xie P, Yang J, Chen J, et al. Advances on materials design and manufacture technology of plastic liner of type IV hydrogen storage vessel. Int J Hydrogen Energy 2022;47:8382–408. <https://doi.org/10.1016/j.ijhydene.2021.12.198>.
- [6] Yersak TA, Baker DR, Yanagisawa Y, Slavik S, Immel R, Mack-Gardner A, et al. Predictive model for depressurization-induced blistering of type IV tank liners for hydrogen storage. Int J Hydrogen Energy 2017;42:28910–7. <https://doi.org/10.1016/j.ijhydene.2017.10.024>.
- [7] Fujiwara H, Ono H, Nishimura S. Degradation behavior of acrylonitrile butadiene rubber after cyclic high-pressure hydrogen exposure. Int J Hydrogen Energy 2015;40:2025–34. <https://doi.org/10.1016/j.ijhydene.2014.11.106>.
- [8] Jung JK, Kim IG, Kim KT. Evaluation of hydrogen permeation characteristics in rubbery polymers. Curr Appl Phys 2021;21:43–9. <https://doi.org/10.1016/j.cap.2020.10.003>.
- [9] Maes C, Molder M te, Luyten W, Herremans G, Winckelmans N, Peeters R, et al. Determination of the nitrogen gas transmission rate (N2GTR) of ethylene vinyl alcohol copolymer, using a newly developed permeation measurement system. Polym Test 2021;93. <https://doi.org/10.1016/j.polymertesting.2020.106979>.
- [10] Fujiwara H, Ono H, Onoue K, Nishimura S. High-pressure gaseous hydrogen permeation test method -property of polymeric materials for high-pressure hydrogen devices (1). Int J Hydrogen Energy 2020;45:29082–94. <https://doi.org/10.1016/j.ijhydene.2020.07.215>.
- [11] Su Y, Lv H, Zhou W, Zhang C. Review of the hydrogen permeability of the liner material of type iv on-board

- hydrogen storage tank. *World Electr Veh J* 2021;12:1–19. <https://doi.org/10.3390/wevj12030130>.
- [12] Kamiya Y, Naito Y, Terada K, Mizoguchi K, Tsuboi A. Volumetric properties and interaction parameters of dissolved gases in poly(dimethylsiloxane) and polyethylene. *Macromolecules* 2000;33:3111–9. <https://doi.org/10.1021/ma991536b>.
- [13] Orme CJ, Stone ML, Benson MT, Peterson ES. Testing of polymer membranes for the selective permeability of hydrogen. *Separ Sci Technol* 2003;38:3225–38. <https://doi.org/10.1081/SS-120022595>.
- [14] Kawamoto S, Fujiwara H, Nishimura S. Hydrogen characteristics and ordered structure of mono-mesogen type liquid-crystalline epoxy polymer. *Int J Hydrogen Energy* 2016; 41:7500–10. <https://doi.org/10.1016/j.ijhydene.2016.03.124>.
- [15] Tocci E, Bellacchio E, Russo N, Drioli E. Diffusion of gases in PEKKs membranes: molecular dynamics simulations. *J Membr Sci* 2002;206:389–98. [https://doi.org/10.1016/S0376-7388\(01\)00784-0](https://doi.org/10.1016/S0376-7388(01)00784-0).
- [16] Kang Y, Cho SM, Kim DK. Charging strategy through analysis of charging influence factors of ultra-light hydrogen storage with polyethylene terephthalate liner. *Int J Hydrogen Energy* 2021;46:9174–85. <https://doi.org/10.1016/j.ijhydene.2021.01.007>.
- [17] Fujiwara H, Ono H, Ohyama K, Kasai M, Kaneko F, Nishimura S. Hydrogen permeation under high pressure conditions and the destruction of exposed polyethylene-property of polymeric materials for high-pressure hydrogen devices (2)-. *Int J Hydrogen Energy* 2021;46:11832–48. <https://doi.org/10.1016/j.ijhydene.2020.12.223>.
- [18] Fujiwara H, Ono H, Nishimura S. Effects of fillers on the hydrogen uptake and volume expansion of acrylonitrile butadiene rubber composites exposed to high pressure hydrogen: -Property of polymeric materials for high pressure hydrogen devices (3)-. *Int J Hydrogen Energy* 2022;47: 4725–40. <https://doi.org/10.1016/j.ijhydene.2021.11.061>.
- [19] Lu H, Li L. Crystalline structure, dielectric, and mechanical properties of simultaneously biaxially stretched polyvinylidene fluoride film. *Polym Adv Technol* 2018;29:3056–64. <https://doi.org/10.1002/pat.4426>.
- [20] Zheng H, Wang B, Zheng G, Wang Z, Dai K, Liu C, et al. Study on crystallization kinetics of partially melting polyethylene aiming to improve mechanical properties. *Ind Eng Chem Res* 2014;53:6211–20. <https://doi.org/10.1021/ie500007n>.
- [21] Ren M, Tang Y, Gao D, Ren Y, Yao X, Shi H, et al. Recrystallization of biaxially oriented polyethylene film from partially melted state within crystallite networks. *Polymer* 2020;191:122291. <https://doi.org/10.1016/j.polymer.2020.122291>.
- [22] Guo P, Xu Y, Lyu M, Zhang S. Fabrication of expanded ethylene-propylene-butene-1 copolymer bead. *Ind Eng Chem Res* 2022;61:2392–402. <https://doi.org/10.1021/acs.iecr.1c04060>.
- [23] Yamabe J, koga A, Nishimura S. Failure behavior of rubber O-ring under cyclic exposure to high-pressure hydrogen gas. *Eng Fail Anal* 2013;35:193–205. <https://doi.org/10.1016/j.engfailanal.2013.01.034>.
- [24] Kulkarni SS, Choi KS, Kuang W, Menon N, Mills B, Soulami A, et al. Damage evolution in polymer due to exposure to high-pressure hydrogen gas. *Int J Hydrogen Energy* 2021;46:19001–22. <https://doi.org/10.1016/j.ijhydene.2021.03.035>.
- [25] Ono H, Fujiwara H, Onoue K, Nishimura S. Influence of repetitions of the high-pressure hydrogen gas exposure on the internal damage quantity of high-density polyethylene evaluated by transmitted light digital image. *Int J Hydrogen Energy* 2019;44:23303–19. <https://doi.org/10.1016/j.ijhydene.2019.07.035>.
- [26] Melnichuk M, Gardavaud Q, Thiébaud F, Perreux D. Numerical assessments of maximum depressurisation rate for polymer materials under high-pressure hydrogen. *Int J Hydrogen Energy* 2021;46:27088–95. <https://doi.org/10.1016/j.ijhydene.2021.05.176>.
- [27] Castagnet S, Mellier D, Nait-Ali A, Benoit G. In-situ X-ray computed tomography of decompression failure in a rubber exposed to high-pressure gas. *Polym Test* 2018;70:255–62. <https://doi.org/10.1016/j.polymertesting.2018.07.017>.
- [28] Yamabe J, Nishimura S. Nanoscale fracture analysis by atomic force microscopy of EPDM rubber due to high-pressure hydrogen decompression. *J Mater Sci* 2011;46:2300–7. <https://doi.org/10.1007/s10853-010-5073-4>.
- [29] Yamabe J, Nishimura S. Influence of fillers on hydrogen penetration properties and blister fracture of rubber composites for O-ring exposed to high-pressure hydrogen gas. *Int J Hydrogen Energy* 2009;34:1977. <https://doi.org/10.1016/j.ijhydene.2008.11.105>. –89.
- [30] Ono H, Fujiwara H, Onoue K, Nishimura S. FT-IR study of state of molecular hydrogen in bisphenol A polycarbonate dissolved by high-pressure hydrogen gas exposure. *Chem Phys Lett* 2020;740. <https://doi.org/10.1016/j.cplett.2019.137053>.
- [31] Gerland M, Boyer SAE, Castagnet S. Early stages of cavitation in a stretched and decompressed poly(vinylidene fluoride) exposed to diffusive hydrogen, observed by Transmission Electronic Microscopy at the nanoscale. *Int J Hydrogen Energy* 2016;41:1766–74. <https://doi.org/10.1016/j.ijhydene.2015.11.015>.
- [32] Einstein A. Über die von der molekularkinetischen Theorie der Wärme geforderte Bewegung von in ruhenden Flüssigkeiten suspendierten Teilchen [AdP 17, 549 (1905)]. *Ann Phys* 1905;14:182–93. <https://doi.org/10.1002/andp.200590005>.
- [33] Shi W, Sorescu DC, Luebke DR, Keller MJ, Wickramanayake S. Molecular simulations and experimental studies of solubility and diffusivity for pure and mixed gases of H₂, CO₂, and Ar absorbed in the ionic liquid 1- n -Hexyl-3-methylimidazolium Bis(Trifluoromethylsulfonyl)amide ([hmim][Tf₂N]). *J Phys Chem B* 2010;114:6531–41. <https://doi.org/10.1021/jp101897b>.
- [34] Yi Y, Bi P, Zhao X, Wang L. Molecular dynamics simulation of diffusion of hydrogen and its isotopic molecule in polystyrene. *J Polym Res* 2018;25:1–6. <https://doi.org/10.1007/s10965-017-1406-1>.
- [35] Lu X, Chen X, Wang YS, Tan YY, Gaomu ZY. Molecular dynamics simulation of gas transport in amorphous polyisoprene. *Wuli Huaxue Xuebao/Acta Phys - Chim Sin* 2016;32:2523–30. <https://doi.org/10.3866/PKU.WHXB201606292>.
- [36] Liu QL, Huang Y. Transport behavior of oxygen and nitrogen through organasilicon-containing polystyrenes by molecular simulation. *J Phys Chem B* 2006;110:17375–82. <https://doi.org/10.1021/jp063174x>.
- [37] Zhao M, Zhang C, Yang F, Weng Y. Gas barrier properties of furan-based polyester films analyzed experimentally and by molecular simulations. *Polymer* 2021;233. <https://doi.org/10.1016/j.polymer.2021.124200>.
- [38] Whitley DM, Adolf DB. Investigating the permeability of atmospheric gases in polyisobutylene membranes via computer simulation. *J Membr Sci* 2012;415–416:260–4. <https://doi.org/10.1016/j.memsci.2012.05.008>.
- [39] Sun B, Lu L, Zhu Y. Molecular dynamics simulation on the diffusion of flavor, O₂ and H₂O molecules in LDPE film. *Materials* 2019;12:10–3. <https://doi.org/10.3390/MA12213515>.
- [40] Cuthbert TR, Wagner NJ, Paulaitis ME, Murgia G, D'Aguanno B. Molecular dynamics simulation of penetrant diffusion in amorphous polypropylene: diffusion

- mechanisms and simulation size effects. *Macromolecules* 1999;32:5017–28. <https://doi.org/10.1021/ma980997e>.
- [41] Liao LQ, Fu YZ, Liang XY, Mei LY, Liu YQ. Diffusion of CO₂ molecules in polyethylene terephthalate/polylactide blends estimated by molecular dynamics simulations. *Bull Kor Chem Soc* 2013;34:753–8. <https://doi.org/10.5012/bkcs.2013.34.3.753>.
- [42] Tamai Y, Tanaka H, Nakanishi K. Molecular simulation of permeation of small penetrants through membranes. 1. Diffusion coefficients. *Macromolecules* 1994;27:4498–508. <https://doi.org/10.1021/ma00094a011>.
- [43] Meunier M. Diffusion coefficients of small gas molecules in amorphous cis-1,4-polybutadiene estimated by molecular dynamics simulations. *J Chem Phys* 2005;123. <https://doi.org/10.1063/1.2049274>.
- [44] Jeyranpour F, Alahyarizadeh G, Minuchehr A. The thermo-mechanical properties estimation of fullerene-reinforced resin epoxy composites by molecular dynamics simulation - a comparative study. *Polymer* 2016;88:9–18. <https://doi.org/10.1016/j.polymer.2016.02.018>.
- [45] Golzar K, Modarress H, Amjad-Iranagh S. Separation of gases by using pristine, composite and nanocomposite polymeric membranes: a molecular dynamics simulation study. *J Membr Sci* 2017;539:238–56. <https://doi.org/10.1016/j.memsci.2017.06.010>.
- [46] Ding M, Szymczyk A, Goujon F, Soldera A, Ghoufi A. Structure and dynamics of water confined in a polyamide reverse-osmosis membrane: a molecular-simulation study. *J Membr Sci* 2014;458:236–44. <https://doi.org/10.1016/j.memsci.2014.01.054>.
- [47] Plimpton S. Fast parallel algorithms for short – range. *Molecular Dynamics* 1995;117:1–42.
- [48] O'Connor TC, Andzelm J, Robbins MO. AIREBO-M: a reactive model for hydrocarbons at extreme pressures. *J Chem Phys* 2015;142:024903. <https://doi.org/10.1063/1.4905549>.
- [49] Noseé S. A unified formulation of the constant temperature molecular dynamics methods. *J Chem Phys* 1984;81:511–9. <https://doi.org/10.1063/1.447334>.
- [50] Hoover WG, Holian BL. Kinetic moments method for the canonical ensemble distribution. *Phys Lett Sect A Gen At Solid State Phys* 1996;211:253–7. [https://doi.org/10.1016/0375-9601\(95\)00973-6](https://doi.org/10.1016/0375-9601(95)00973-6).
- [51] Stukowski A. Visualization and analysis of atomistic simulation data with OVITO-the Open Visualization Tool. *Model Simulat Mater Sci Eng* 2010;18. <https://doi.org/10.1088/0965-0393/18/1/015012>.
- [52] Rutherford SW, Limmer DT, Smith MG, Honnell KG. Gas transport in ethylene-propylene-diene (EPDM) elastomer: molecular simulation and experimental study. *Polymer* 2007;48:6719–27. <https://doi.org/10.1016/j.polymer.2007.07.020>.
- [53] Sudibjo A, Spearot DE. Molecular dynamics simulation of diffusion of small atmospheric penetrates in polydimethylsiloxane. *Mol Simulat* 2011;37:115–22. <https://doi.org/10.1080/08927022.2010.524646>.
- [54] Kremer K, Grest GS. Dynamics of entangled linear polymer melts: a molecular-dynamics simulation. *J Chem Phys* 1990;92:5057. <https://doi.org/10.1063/1.458541>.
- [55] Tan JH, Chen CL, Liu YW, Wu JY, Wu D, Zhang X, et al. Molecular simulations of gas transport in hydrogenated nitrile butadiene rubber. *J Polym Res* 2020;27. <https://doi.org/10.1007/s10965-020-02258-3>.
- [56] Mason EA, Rice WE. The intermolecular potentials of helium and hydrogen. *J Chem Phys* 1954;22:522–35. <https://doi.org/10.1063/1.1740100>.
- [57] Hossain D, Tschoop MA, Ward DK, Bouvard JL, Wang P, Horstemeyer MF. Molecular dynamics simulations of deformation mechanisms of amorphous polyethylene. *Polymer* 2010;51:6071–83. <https://doi.org/10.1016/j.polymer.2010.10.009>.
- [58] Shang Y, Zhang X, Xu H, Li J, Jiang S. Microscopic study of structure/property interrelation of amorphous polymers during uniaxial deformation : a molecular dynamics approach. *Polymer* 2015;77:254–65. <https://doi.org/10.1016/j.polymer.2015.09.017>.
- [59] Bao Q, Yang Z, Lu Z. Molecular dynamics simulation of amorphous polyethylene (PE) under cyclic tensile-compressive loading below the glass transition temperature. *Polymer* 2020;186:121968. <https://doi.org/10.1016/j.polymer.2019.121968>.
- [60] Zhang Z, Handa YP. An in situ study of plasticization of polymers by high-pressure gases. *J Polym Sci, Part B: Polym Phys* 1998;36:977–82. [https://doi.org/10.1002/\(SICI\)1099-0488\(19980430\)36:6<977.AID-POLB5>3.0.CO;2-D](https://doi.org/10.1002/(SICI)1099-0488(19980430)36:6<977.AID-POLB5>3.0.CO;2-D).
- [61] Cha JH, Lee W, Baek J. Penetration of hydrogen into polymer electrolyte membrane for fuel cells by quantum and molecular dynamics simulations. *Polymers* 2021;13. <https://doi.org/10.3390/polym13060947>.
- [62] Kontopoulou M, Vlachopoulos J. Bubble dissolution in molten polymers and its role in rotational molding. *Polym Eng Sci* 1999;39:1189–98. <https://doi.org/10.1002/pen.11505>.
- [63] Flaconneche B, Martin J, Klopffer MH. Permeability, diffusion and solubility of gases in polyethylene, polyamide 11 and poly (vinylidene fluoride). *Oil Gas Sci Technol* 2001;56:261–78. <https://doi.org/10.2516/ogst:2001023>.
- [64] Yuan Z, Lu Z, Yang Z, Sun J, Xie F. A criterion for the normal properties of graphene/polymer interface. *Comput Mater Sci* 2016;120:13–20. <https://doi.org/10.1016/j.commatsci.2016.04.006>.
- [65] Jin Y, Duan F, Mu X. Functionalization enhancement on interfacial shear strength between graphene and polyethylene. *Appl Surf Sci* 2016;387:1100–9. <https://doi.org/10.1016/j.apsusc.2016.07.047>.
- [66] Bandyopadhyay P, Nguyen TT, Li X, Kim NH, Lee JH. Enhanced hydrogen gas barrier performance of diaminoalkane functionalized stitched graphene oxide/polyurethane composites. *Compos B Eng* 2017;117:101–10. <https://doi.org/10.1016/j.compositesb.2017.02.035>.
- [67] Ebina T, Ishii R, Aizawa T, Yoshida H. Development of clay-based film and its application to gas barrier layers of composite tanks. *J Japan Pet Inst* 2017;60:121–6. <https://doi.org/10.1627/jpi.60.121>.
- [68] Duncan TV. Applications of nanotechnology in food packaging and food safety: barrier materials, antimicrobials and sensors. *J Colloid Interface Sci* 2011;363:1–24. <https://doi.org/10.1016/j.jcis.2011.07.017>.
- [69] Zhao H, Zhang Q, Ali S, Li L, Lv F, Ji Y, et al. A real-time WAXS and SAXS study of the structural evolution of LLDPE bubble. *J Polym Sci, Part B: Polym Phys* 2018;56:1404–12. <https://doi.org/10.1002/polb.24727>.